be lowered by 20–40 cm^{-1}, depending on the level of theory used and the nature of the substituent. The effect of replacing only one oxygen with a heavy isotope is approximately half that of replacing both, as would be expected for an O–O stretch.

Conclusion

The reactions of singlet oxygen with H_2S and Me_2S have been calculated by ab initio methods. A peroxy sulfoxide structure is found to be a stable, but weakly bound, intermediate. This result supports the mechanism proposed for the photooxidation of organic sulfides. A second proposed intermediate, a cyclic thiadioxirane, is found to be a local maximum on the potential energy surface and is not a valid intermediate. Large-scale MCSCF results show that the peroxy sulfoxide is best described by a zwitterionic and not a biradical structure. Activation energies and overall heats of reaction are very sensitive to the quality of the basis set. When additivity of the effects of improving the basis set and inclusion of electron correlation are assumed, the activation energy for the formation of dimethyl peroxy sulfoxide at the MP2/6-311G(3d) level is estimated to be ~10 kcal/mol. This is 5–10 kcal/mol higher than experimentally observed and suggests that even higher level calculations are necessary. The formation of a solvent adduct in protic solvents from the peroxy sulfoxide (a sulfurane) is calculated to be approximately thermoneutral, although an accurate prediction is difficult from the present calculations. The infrared spectrum and isotopic shifts of the peroxy sulfoxide have been calculated for possible spectroscopic identification.

After this work was completed, Ando et al.[42] reported IR spectra of a reactive intermediate formed upon irradiation of a sulfide in an oxygen matrix at 13 K. The intermediate formed from diphenyl sulfide has an IR absorption at 997 cm^{-1}, which is shifted to 978 cm^{-1} when $^{18}O^{18}O$ is used and split into two bands at 993 and 984 cm^{-1} when $^{18}O^{16}O$ is used. These data agree reasonably well with the calculated values in this work. If the observed intermediate is indeed a peroxy sulfoxide, the calculations predict that there should be another strong IR band at ~910 cm^{-1} (only the region 960–1040 cm^{-1} was reported in ref 42), which should show a characteristic frequency shift upon isotopic substitution.

Acknowledgment. We thank Exxon for a fellowship, the Friedman Bag Co. for additional support (F.J.), and the San Diego Supercomputer Center for computer time. We also thank Professor K. N. Houk for helpful discussions. This work was supported by National Science Foundation Grant No. CHE86-11873.

(42) Akasaka, T.; Yabe, A.; Ando, W. *J. Am. Chem. Soc.* **1987**, *109*, 8085. We thank Prof. Ando for a preprint of this manuscript.

Remarkable Stabilities of the Diatomic Multiply Charged Cations $SiHe^{\cdot 3+}$ and $SiHe^{4+}$

Ming Wah Wong and Leo Radom*

Contribution from the Research School of Chemistry, Australian National University, Canberra, A.C.T. 2601, Australia. *Received October 9, 1987*

Abstract: Ab initio molecular orbital theory using basis sets up to 6-311G(MC)(2d,2p) and with electron correlation incorporated at the fourth-order Møller–Plesset level has been used to study the series of diatomic ions $SiHe^{n+}$ (n = 1–4). The $SiHe^{\cdot +}$ monocation and $SiHe^{2+}$ dication are found to be weakly bound species with long silicon–helium bonds. On the other hand, the $SiHe^{\cdot 3+}$ trication and $SiHe^{4+}$ tetracation are characterized by considerably shorter Si–He bonds (1.670 and 1.550 Å, respectively). In spite of the availability of extremely exothermic fragmentation processes, $SiHe^{\cdot 3+}$ and $SiHe^{4+}$ are predicted to be potentially observable species in the gas phase. The trend of Si–He bond lengths in the series of $SiHe^{n+}$ ions can readily be understood in terms of the number of electrons occupying antibonding orbitals. $SiHe^{4+}$, with just two valence electrons, is the smallest stable polyatomic tetracation yet reported in the literature.

The chemistry of helium-containing cations[1] has attracted increasing recent interest. In spite of the chemical inertness of the helium atom, many helium-containing ions are predicted to be stable and to contain strong bonds to helium. Indeed, several such ions have recently been observed in mass spectrometry experiments.[2] Most studies of helium-containing ions to date have dealt mainly with singly charged or doubly charged species. In recent theoretical investigations, however, we have shown[3] that even highly charged ions, CHe_4^{4+}, $CHe_3^{\cdot 3+}$, and $HeCF^{3+}$, display remarkable stability despite extreme coulomb repulsion. In this paper, we present evidence for the stability of the *diatomic* tri- and tetracations, $SiHe^{\cdot 3+}$ and $SiHe^{4+}$. Results are reported for the series of diatomic ions $SiHe^{n+}$ (n = 1–4) and rationalized in terms of a simple orbital interaction model.[4]

Method and Results

Standard ab initio molecular orbital calculations were carried out with a modified version[5] of the Gaussian 82 system of programs.[6] Geometry optimizations for all systems were performed with the triple-split-valence plus dp-polarization 6-311G(MC)** basis set[7-9] and valence-electron correlation incorporated at the

(1) For leading references, see: (a) Cooper, D. L.; Wilson, S. *Mol. Phys.* **1981**, *44*, 161. (b) Schleyer, P. v. R. *Adv. Mass Spectrom.* **1985**, 287. (c) Koch, W.; Frenking, G.; Gauss, J.; Cremer, D.; Collins, J. R. *J. Am. Chem. Soc.* **1987**, *109*, 5917. (d) Wong, M. W.; Bürgi, H. B.; Radom, L., to be published.

(2) For example, see: (a) Guilhaus, M.; Brenton, A. G.; Beynon, J. H.; Rabrenovic, M.; Schleyer, P. v. R. *J. Chem. Soc., Chem. Commun.* **1985**, 210. (b) Young, S. E.; Coggiola, M. J. *Int. J. Mass Spectrom. Ion Proc.* **1986**, *74*, 137.

(3) (a) Wong, M. W.; Nobes, R. H.; Radom, L. *J. Chem. Soc., Chem. Commun.* **1987**, 233. (b) Wong, M. W.; Nobes, R. H.; Radom, L. *Rapid Commun. Mass Spectrom.* **1987**, *1*, 3.

(4) Our more general qualitative rationalization of the unusual structural features of helium-containing cations will be presented elsewhere;[1d] a related approach is described in the excellent paper of Koch, Frenking, et al.[1c]

(5) (a) Baker, J.; Nobes, R. H.; Wong, M. W., unpublished. (b) Baker, J. *J. Comput. Chem.* **1986**, *7*, 385. (c) Baker, J. *J. Comput. Chem.* **1987**, *8*, 563.

(6) Binkley, J. S.; Frisch, M. J.; DeFrees, D. J.; Raghavachari, K.; Whiteside, R. A.; Schlegel, H. B.; Fluder, E. M.; Pople, J. A. GAUSSIAN 82, Carnegie-Mellon University, Pittsburgh, PA 15213.

0002-7863/88/1510-2375$01.50/0

Table I. Calculated Total Energies[a] (hartrees), Zero-Point Vibrational Energies (ZPVE, kJ mol^{-1}), and Relative Energies[a] (kJ mol^{-1}) for $SiHe^{n+}$ Structures and Related Species

species	state	total energy: MP3/6-311G-(MC)**[b]	total energy: MP4/6-311G-(MC)(2d,2p)[c]	ZPVE	relative energy: MP3/6-311G-(MC)**	relative energy: MP4/6-311G-(MC)(2d,2p)	relative energy: MP4/6-311G-(MC)(2d,2p)[d]
$SiHe^{\cdot+}$ (**1**)	$^2\Pi$	−291.51074	−291.52290	0.5	0	0	0
$SiHe^{\cdot+}$ (**2**)	$^4\Sigma^-$	−291.33772	−291.34732	1.7	454	461	462
$Si^{\cdot+}$ + He		−291.51045	−291.52232	0	1	2	1
$SiHe^{2+}$ (**3**)	$^1\Sigma^+$	−290.92285	−290.93242	0.8	0	0	0
$SiHe^{2+}$ (**4**)	$^3\Pi$	−290.70949	−290.71721	3.5	560	565	568
Si^{2+} + He		−290.92122	−290.92871	0	4	10	9
$Si^{\cdot+}$ + $He^{\cdot+}$		−290.61612	−290.62337	0	805	811	810
$SiHe^{\cdot 3+}$ (**5**)	$^2\Sigma^+$	−289.74904	−289.75597	4.8	0	0	0
TS: **5** → Si^{2+} + $He^{\cdot+}$ (**6**)	$^2\Sigma^+$	−289.71010	−289.71638	0	102	104	100
Si^{2+} + $He^{\cdot+}$		−290.02689	−290.02976	0	−729	−719	−724
$Si^{\cdot 3+}$ + He		−289.70728	−289.71190	0	110	116	111
$SiHe^{4+}$ (**7**)	$^1\Sigma^+$	−288.19413	−288.20068	6.8	0	0	0
TS: **7** → $Si^{\cdot 3+}$ + $He^{\cdot+}$ (**8**)	$^1\Sigma^+$	−288.14507	−288.16936	0	141	82	76
$Si^{\cdot 3+}$ + $He^{\cdot+}$		−288.81295	−288.81295	0	−1625	−1608	−1614
Si^{4+} + He		−288.06706	−288.07168	0	334	339	332

[a] MP3/6-311G(MC)** optimized structures. [b] Calculated MP3/6-311G(MC)** total energies include −288.61798 ($Si^{\cdot+}$,^{2}P), −288.02875 (Si^{2+},^{1}P), −286.81481 ($Si^{\cdot 3+}$,^{2}S), −285.17459 (Si^{4+},^{1}S), −2.89247 (He,^{1}S), and −1.99814 ($He^{\cdot+}$,^{2}S). [c] Calculated MP4/6-311G(MC)(2d,2p) total energies include −288.62523 ($Si^{\cdot+}$,^{2}P), −288.03162 (Si^{2+},^{1}P), −286.81481 ($Si^{\cdot 3+}$,^{2}S), −285.17459 (Si^{4+},^{1}S), −2.89709 (He,^{1}S), and −1.99814 ($He^{\cdot+}$,^{2}S). [d] Including zero-point vibrational correction.

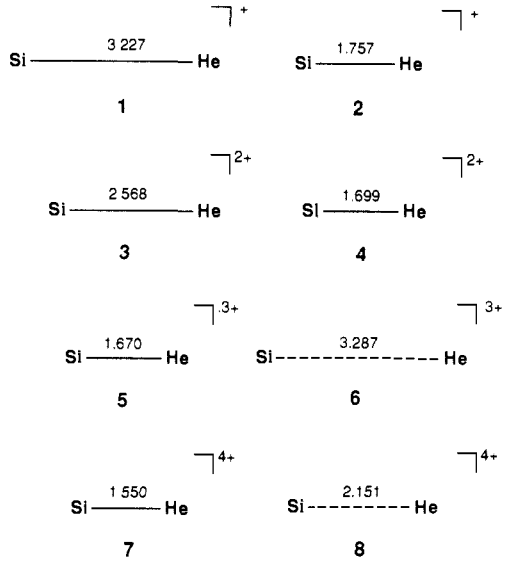

Figure 1. Optimized structures (MP3/6-311G(MC)**) for $SiHe^{n+}$ cations.

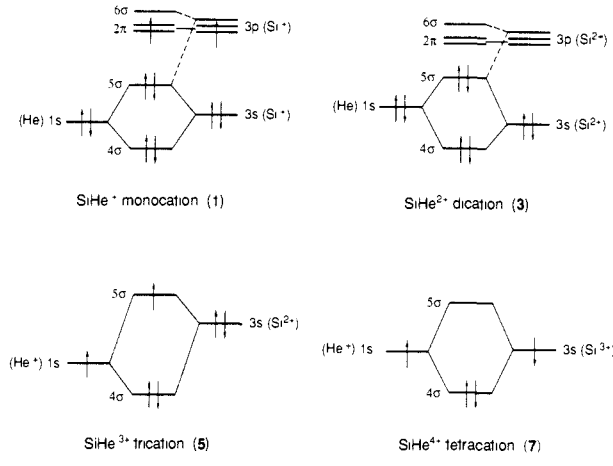

Figure 2. Orbital interaction diagrams for $SiHe^{n+}$ cations.

third-order Møller–Plesset level (MP3).[10] Harmonic frequencies were calculated at the MP2/6-31G*[10,11] level in order to characterize stationary points as minima or saddle points and to determine zero-point vibrational energies (ZPVE). The directly calculated ZPVEs were scaled by a factor of 0.93[12] for the latter purpose. Improved relative energies were obtained from full fourth-order Møller–Plesset (MP4) calculations[13] with the 6-311G(MC)(2d,2p)[7] basis set based on the MP3/6-311G(MC)** optimized structures. Unless otherwise noted, spin-restricted calculations (RHF, RMP) were used for closed-shell systems and spin-unrestricted calculations (UHF, UMP) for open-shell systems. We have previously found it preferable to use RMP4 rather than UMP4 for energy comparisons in cases where the UHF wave function is significantly spin-contaminated.[14,15] Accordingly, in the present study, we have used an RMP4 energy calculation in conjunction with the UMP3 geometry for transition structure **8** for which the spin-squared expectation value $\langle S^2 \rangle$ is 0.66 (UHF/6-311G(MC)**). No other cases of significant spin contamination were encountered. Unless otherwise stated, relative energies refer to MP4/6-311G(MC)(2d,2p) values, corrected for zero-point vibrational contributions, and structural parameters to MP3/6-311G(MC)** values. The full set of $SiHe^{n+}$ structures is displayed in Figure 1, and their calculated total energies and relative energies are shown in Table I. Bond lengths throughout this paper are in angstroms. The frozen-core approximation was employed in all calculations.

Discussion

$SiHe^{\cdot+}$ Monocation. The $^2\Pi$ ground state (**1**) of $SiHe^{\cdot+}$ monocation is characterized by a very long bond (3.227 Å) and a calculated dissociation energy for the process $SiHe^{\cdot+}$ → $Si^{\cdot+}$ + He of only 1 kJ mol^{-1}. The first excited $^4\Sigma^-$ state of $SiHe^{\cdot+}$ (**2**) lies 462 kJ mol^{-1} above **1** but has a rather short Si–He bond

(7) The 6-311G(MC)** basis set employs as underlying basis sets the standard 6-311G basis set[8] for H, He, and first-row atoms, and the (12s,9p) → [6s,5p] McLean–Chandler (MC) basis set[9] for second-row atoms. The polarization function exponents for H and first-row atoms have standard values; those for He and the second-row atoms were chosen on the basis of exponent optimizations for the normal-valent hydrides. Full details are provided in: Wong, M. W.; Gill, P. M. G.; Nobes, R. H.; Radom, L. *J. Phys. Chem.*, in press.

(8) Krishnan, R.; Binkley, J. S.; Seeger, R.; Pople, J. A. *J. Chem. Phys.* **1980**, *72*, 650.

(9) McLean, A. D.; Chandler, G. S. *J. Chem. Phys.* **1980**, *72*, 5639.

(10) (a) Møller, C.; Plesset, M. S. *Phys. Rev.* **1934**, *46*, 618. (b) Pople, J. A.; Binkley, J. S.; Seeger, R. *Int. J. Quantum Chem. Symp.* **1976**, *10*, 1.

(11) (a) Hehre, W. J.; Ditchfield, R.; Pople, J. A. *J. Chem. Phys.* **1972**, *56*, 2257. (b) Hariharan, P. C.; Pople, J. A. *Theor. Chim. Acta* **1973**, *28*, 213.

(12) Hout, R. F.; Levi, B. A.; Hehre, W. J. *J. Comput. Chem.* **1982**, *3*, 234.

(13) Krishnan, R.; Frisch, M. J.; Pople, J. A. *J. Chem. Phys.* **1980**, *72*, 4244.

(14) Gill, P. M. W.; Radom, L. *Chem. Phys. Lett.* **1986**, *132*, 16.

(15) Gill, P. M. W.; Wong, M. W.; Nobes, R. H.; Radom, L., to be published.

length, 1.757 Å. The differences between the geometries of **1** and **2** are striking.

The dramatic shortening of the Si–He bond distance in going from the doublet state to the quartet state may be understood by considering the interaction between the orbitals of the separated fragments. Interaction of the He 1s atomic orbital with the $Si^{\bullet+}$ 3s atomic orbital produces two molecular orbitals: a bonding orbital (4σ) and an antibonding orbital (5σ) (Figure 2). In addition, the $Si^{\bullet+}$ $3p_\sigma$ orbital mixes into 5σ in a bonding manner. The extent of such mixing is small, however, because of the relatively large energy gap between the interacting orbitals. The remaining 3p orbitals on $Si^{\bullet+}$ give rise to a degenerate pair of nonbonding π orbitals (2π). Of the five valence electrons in the ground state (**1**) of $SiHe^{\bullet+}$, two occupy the 4σ (bonding) orbital, two occupy the 5σ (antibonding) orbital, and one occupies the 2π (nonbonding) orbital. Double occupation of the antibonding orbital means that there is very little net bonding and results in a long Si–He bond in ground-state $SiHe^{\bullet+}$. When going from the doublet state (**1**) to the quartet state (**2**), one of the electrons in the antibonding 5σ orbital is promoted to one of the nonbonding 2π orbitals. Although this is energetically costly, it leads to a substantial shortening of the Si–He distance. In several recent studies,[1c,16,17] Koch and Frenking have also noted that the geometries of helium-containing ions depend strongly on the electronic state of the system.

$SiHe^{2+}$ Dication. As in the monocation, the Si–He bond in the $^1\Sigma^+$ ground state (**3**) of the $SiHe^{2+}$ dication is rather long (2.568 Å). The Löwdin population analysis shows that the Si^{2+} moiety has gained just 0.05 e from the He atom at the equilibrium bond distance of $SiHe^{2+}$, i.e., the ground-state equilibrium structure of $SiHe^{2+}$ resembles Si^{2+} weakly bonded to He. The triplet state (**4**) has a much shorter Si–He bond length (1.699 Å) but a much higher energy, 568 kJ mol^{-1} above **3**. In a similar manner to that of the $SiHe^{\bullet+}$ monocation, the shortening of the Si–He distance in the triplet structure (**4**) may be attributed largely to the removal of one of the antibonding 5σ-electrons of the singlet structure (**3**).

Since the second ionization energy of silicon (1559 kJ mol^{-1}) is lower than the first ionization energy of helium (2360 kJ mol^{-1}),[18] dissociation to Si^{2+} + He is the most favorable fragmentation pathway for **3**. The calculated barrier for such a fragmentation is less than 10 kJ mol^{-1} so that the ground-state equilibrium structure of $SiHe^{2+}$ is unlikely to be experimentally accessible.

$SiHe^{\bullet3+}$ Trication. The $SiHe^{\bullet3+}$ trication is found to be more strongly bound than its singly charged and doubly charged counterparts. The $^2\Sigma^+$ ground state (**5**) has a minimum at a relatively short Si–He distance, 1.670 Å. The bonding situation in this case is more favorable than that for the ground states of $SiHe^{\bullet+}$ and $SiHe^{2+}$, the 5σ-antibonding orbital being only singly occupied, and this contributes to the shorter Si–He bond length in the $SiHe^{\bullet3+}$ trication.

Fragmentation of **5** to Si^{2+} + $He^{\bullet+}$ is highly exothermic (by 724 kJ mol^{-1}). However, this dissociation, via transition structure **6**, is inhibited by an energy barrier of 100 kJ mol^{-1}. The $SiHe^{\bullet3+}$ trication is therefore potentially observable in the gas phase. It could perhaps be generated through collision of the $Si^{\bullet3+}$ trication with helium.

Interestingly, the bond length of the transition structure **6** is rather long, being approximately twice that of the equilibrium structure (**5**). In a recent paper, Gill and Radom[19] provided a rationalization of the transition structure bond lengths for a number of representative dication fragmentations. In particular, for dications with late transition structures, they provided a simple formula to estimate the length of the breaking bond in the transition structure, based solely on a knowledge of the ionization energies of the fragments. We present here the straightforward extension to fragmentations of more highly charged ions.

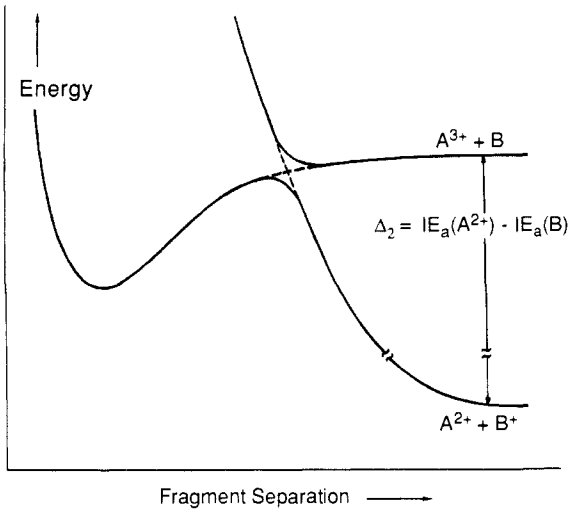

Figure 3. Schematic potential energy curves for a general AB^{3+} trication showing avoided crossing between A^{3+} + B and A^{2+} + B^+ diabatic potentials.

For a dissociating trication AB^{3+}, the potential energy curve along the reaction coordinate can be considered as arising from an avoided crossing between a repulsive state which correlates with A^{2+} + B^+ and an attractive state which correlates with A^{3+} + B (Figure 3). For sufficiently late transition structures, the estimated transition structure bond length (r_{TS}), as represented approximately by the crossing point, is given by

$$r_{TS} = 2/\Delta_2 \quad (\Delta_2 \text{ and } r_{TS} \text{ in au}) \qquad (1)$$

where Δ_2 is the difference between the adiabatic ionization energies (IE_a) of A^{2+} and B. For the case of $SiHe^{\bullet3+}$, eq 1 predicts[20] a transition structure bond length of 3.24 Å, in good agreement with the directly calculated MP3/6-311G(MC)** value of 3.29 Å.

$SiHe^{4+}$ Tetracation. The Si–He bond length calculated for the $^1\Sigma^+$ ground state (**7**) of the $SiHe^{4+}$ tetracation is the shortest in the $SiHe_n^{n+}$ series and comparable to that of a normal Si–H bond (e.g., 1.481 Å in SiH_4).[21] This short Si–He bond can readily be explained in terms of the empty 5σ-antibonding molecular orbital in **7** (Figure 2).

How stable is the $SiHe^{4+}$ tetracation? The exothermicity of the fragmentation to $Si^{\bullet3+}$ + $He^{\bullet+}$ is enormous: 1615 kJ mol^{-1}. However, the barrier for such a process, 76 kJ mol^{-1}, is sufficiently large that we believe experimental observation will be feasible.

Finally, the bond length in the $SiHe^{4+}$ fragmentation transition structure may be estimated by using a formula analogous to that given previously for dications[19] and given in eq 1 above for trications. Thus, for a dissociating AB^{4+} tetracation for which A^{3+} + B^+ lies lower in energy than A^{2+} + B^{2+}, the potential energy curve along the reaction coordinate can be considered as arising from an avoided crossing between a repulsive state which correlates with A^{3+} + B^+ and an attractive state which correlates with A^{4+} + B. The estimated transition structure bond length is then given by

$$r_{TS} = 3/\Delta_3 \qquad (2)$$

where Δ_3 is the difference between the adiabatic ionization energies (IE_a) of A^{3+} and B. For $SiHe^{4+}$, the value of r_{TS} from eq 2[20] is 2.10 Å compared with the directly calculated value of 2.15 Å.

Concluding Results

Several important points emerge from this study:

(1) Consistent with our previous findings for the CHe_n^{n+} ions, it is the more highly charged trication and tetracation in the series

(16) Koch, W.; Frenking, G. *J. Chem. Soc., Chem. Commun.* **1986**, 1095.
(17) Koch, W.; Frenking, G.; Luke, B. T. *Chem. Phys. Lett.* **1987**, *139*, 149.
(18) Corresponding experimental ionization energies for $Si^{\bullet+}$ and He are 1577 and 2372 kJ mol^{-1}, respectively: Weast, R. C. *CRC Handbook of Chemistry and Physics*, 67th ed.; CRC Press: FL, 1986.
(19) Gill, P. M. W.; Radom, L. *Chem. Phys. Lett.* **1987**, *136*, 294.
(20) Calculated with use of experimental ionization energies from ref 18.
(21) Chase, M. W.; Curnutt, J. L.; McDonald, R. A.; Syverud, A. N. JANAF Thermochemical Tables, 1978 Supplement, *J. Phys. Chem. Ref. Data* **1978**, *7*, 793.

of $SiHe^{n+}$ ions which display the strongest Si-He bonds and the greatest kinetic stability.

(2) In spite of the availability of extremely exothermic fragmentation processes, both the $SiHe^{\bullet 3+}$ trication and $SiHe^{4+}$ tetracation are predicted to be potentially accessible species in the gas phase.

(3) The trends in the Si-He bond lengths in the series $SiHe^{n+}$ can readily be rationalized in terms of the number of electrons occupying the 5σ-antibonding molecular orbital.

(4) $SiHe^{4+}$, with just two valence electrons, is the smallest stable polyatomic tetracation yet reported in the literature.

Acknowledgment. We thank Peter Gill and Dr. Ross Nobes for helpful and stimulating discussions and Dr. Gernot Frenking for a preprint of ref 1c.

Registry No. $SiHe^{\bullet 3+}$, 113161-95-8; $SiHe^{4+}$, 113161-96-9; Si, 7440-21-3; He, 7440-59-7.

Determination of ^{15}N Chemical Shift Tensor via ^{15}N-^{2}H Dipolar Coupling in Boc-glycylglycyl[^{15}N]glycine Benzyl Ester

Yukio Hiyama,[†,∥] Chien-Hua Niu,[§] James V. Silverton,[‡] Alfonso Bavoso,[‡,⊥] and Dennis A. Torchia*[†]

Contribution from the Bone Research Branch, National Institute of Dental Research, Laboratory of Chemistry, National Heart, Lung, and Blood Institute, and Laboratory of Experimental Carcinogenesis, National Cancer Institute, National Institutes of Health, Bethesda, Maryland 20892. *Received May 28, 1987*

Abstract: Proton-decoupled ^{15}N nuclear magnetic resonance line shapes of two crystalline phases of Boc-glycylglycyl[^{15}N,^{2}H]glycine benzyl ester are reported. Analysis of the spectra shows that ^{15}N-^{2}H bond distances are 1.042 and 1.050 Å, respectively, in the two phases and that the z axes of the chemical shift tensors make angles of 22° and 24° with respect to the N-H bond axis in each phase. In one phase the shift anisotropy is 168 ppm, and the asymmetry parameter has a small value, $\eta = 0.064$, typical of a peptide nitrogen. In contrast, an unusually large value of η, 0.44, is observed in the other phase of the peptide. Measurements of ^{15}N and ^{2}H relaxation times show that the difference in η values does not arise from molecular motion while measurements of ^{2}H quadrupole coupling constants indicate that hydrogen bond geometry is nearly the same in the two phases. X-ray diffraction shows that the phase having $\eta = 0.44$ has a triclinic lattice (a = 6.107 (3), b = 9.145 (4), c = 18.832 (2) Å; α = 76.36 (2), β = 85.42 (2), γ = 75.62 (4)°), while the phase having $\eta = 0.064$ has a monoclinic lattice (a = 13.228 (1), b = 9.259 (1), c = 17.118 (1) Å; β = 102.15 (1)°). Although only the monoclinic crystals were suitable for a complete structure determination, these differences in lattice and unit cell dimensions strongly suggest that the peptide assumes different conformations in the two phases. We discuss the possibility that a nonplanar peptide is the cause of the large asymmetry observed in the triclinic phase.

Solid-state ^{15}N NMR (nuclear magnetic resonance) spectroscopy has proven to be a useful tool for investigating the structure of fibrous proteins, where X-ray crystallography provides incomplete structural information.[1] The NMR studies, however, require thorough knowledge of the nitrogen chemical shift tensor: principal elements and their orientations. The orientation of the z principal axis of the ^{15}N chemical shift tensor of the peptide nitrogen in a single crystal of glycylglycine hydrochloride monohydride has been determined.[2] However, the minor principal axes' orientations were not determined[2] because of the commonly observed small asymmetry parameter (less than 0.1).

Herein, we report the orientations of ^{15}N chemical shift tensors in two crystalline forms of Boc-glycylglycyl[^{15}N,^{2}H]glycine benzyl ester. The shift tensor orientations were determined relative to the ^{15}N-^{2}H bond axis by analysis of proton-decoupled ^{15}N powder line shapes. In addition, we report values of ^{15}N-^{2}H bond distances, also obtained from the line shape analysis, and hydrogen bond distances obtained from measurements of ^{2}H quadrupole coupling constants.

A surprising observation was the large value of the asymmetry parameter ($\eta = 0.44$) obtained for one crystalline phase of the peptide. This large asymmetry is atypical of peptide nitrogen shift tensors, which normally have $\eta \leq 0.1$, as was found for the other crystalline form of $Boc(Gly)_3OBz$. X-ray diffraction showed that the peptide having $\eta = 0.44$ has a triclinic lattice while the $\eta = 0.064$ crystals have a monoclinic lattice. Although only the monoclinic crystals were suitable for a complete structure determination, unit cell parameters were determined for both crystalline forms and suggested that the difference in η resulted from differences in peptide conformations. In agreement with this conclusion, NMR relaxation measurements show that the differences in η do not arise from differences in molecular motion in the crystalline phases. We discuss possible conformational characteristics that could give rise to the large chemical shift asymmetry observed in the triclinic phase.

Experimental Section

$Boc(Gly)_3OBz$ was synthesized in the manner reported previously.[3] The triclinic phase of the peptide was recrystallized within 1 min by blowing nitrogen gas from a saturated dry (Na_2SO_4 anhydrous) ethyl acetate solution. The monoclinic phase was obtained from any one of the following solutions: wet ethyl acetate, chloroform, ethanol, or dry ethyl acetate with slow recrystallization. N-Deuteriated triclinic crystals were prepared by exchange in ethyl acetate/D_2O. Deuteriated monoclinic crystals were prepared by exchange in EtOD and were found to

[†] National Institute of Dental Research.
[‡] National Heart, Lung, and Blood Institute.
[§] National Cancer Institute.
[∥] Permanent address: Upjohn Pharmaceuticals Ltd., Nishi Shinjuku, Tokyo 160, Japan.
[⊥] Permanent address: Universita di Napoli, Dipartmento di Chemica, Via Mezzocannone 4, 80134, Naples, Italy.

(1) Cross, T. A.; Opella, S. J. *J. Mol. Biol.* **1985**, *182*, 367-381.
(2) Harbison, G. S.; Jelinski, L. W.; Stark, R. E.; Torchia, D. A.; Herzfeld, J.; Griffin, R. G. *J. Magn. Reson.* **1984**, *60*, 79-82.
(3) Niu, C.-H.; Black, S. *J. Biol. Chem.* **1979**, *254*, 265-267.

0002-7863/88/1510-2378$01.50/0